Optical second harmonic generation from V-shaped chromium nanohole arrays

Ngo Khoa Quang[1], Yoshihiro Miyauchi[2], Goro Mizutani[1,*], Martin D. Charlton[3], Ruiqi Chen[3], Stuart Boden[3], and Harvey Rutt[3]

[1]School of Materials Science, Japan Advanced Institute of Science and Technology, 1-1 Asahidai, Nomi, Ishikawa 923-1292, Japan

[2]Department of Applied Physics, National Defense Academy, Hashirimizu 1-10-20, Yokosuka-shi, Kanagawa 239-8686, Japan

[3]School of Electronics and Computer Science, University of Southampton, SO17 1BJ, UK

[*]E-mail: mizutani@jaist.ac.jp

We observed rotational anisotropy of optical second harmonic generation (SHG) from an array of V-shaped chromium nanoholes fabricated by electron beam lithography. Phenomenological analysis indicated that the effective nonlinear susceptibility element $\chi_{313}^{(2)}$ had a characteristic contribution to the observed anisotropic SHG intensity patterns. Here, coordinate 1 is in the direction of the tip of V shapes in the substrate plane, and 3 indicates the direction perpendicular to the sample surface. The SHG intensity for the S-polarized output light was very weak, probably owing to the cancellation effect of the image dipoles generated at the metal-air boundary. The possible origin of the observed nonlinearity is discussed in terms of the susceptibility elements obtained.

1. Introduction

Metamaterials have many intriguing features and are currently intensively researched[1)]. At the nanoscale, artificial structures tend to show unusual characteristics, such as negative electric permittivity[2)], optical cloaks[2)], super lensing[3)], and many more[4-8)]. Among artificial nanostructures, nanohole arrays exhibit many interesting features in terms of nonlinear optics[1,9-13)]. Airola et al.[9)] showed an enhancement of the transmitted second harmonic generation (SHG) signal in a periodic circular nanohole array owing to the enhanced transmission of the incident light. They found an enhanced SHG from disordered circular gold nanohole arrays compared with periodic arrays. More recently, it has been found that the overlapping of two circular holes induced an enhancement of SHG by as much as 14 times compared with circular holes, owing to a strong local field at the sharp apexes inside the overlapping holes[13,14)]. Not only the resonant enhancement of the SHG but also the polarized linear optical response of the overlapping double holes are sensitive to the hole structure because of the localized surface plasmon excitation at the apex tips[13)].

In the above-mentioned works, gold or silver was adopted as the substrate material because they are favorable for plasmon excitation[15,16)]. Chromium is usually employed as an adhesion layer[14,16)] before depositing a gold or silver thin film and shaping the nanoholes. Nevertheless, a quick calculation shows that the "sensible observability for a surface plasmon resonance" defined by Sambles et al.[17)] and Sarid and Challener[18)] is smaller than 0.1 for wavelengths from 400 to 1200 nm. According to Sambles et al.[17)], a sensible observability value smaller than 0.2 permits surface plasmon resonance. Indeed, Shalabney et al. found surface plasmon resonance in Cr

columnar thin films in the Kretschmann configuration[19]. This requires us to clarify plasmon excitation in chromium metal in more detail for plasmonic device applications[20]. Hence, our concern in this study is to check whether plasmon excitation emerges in a nonlinear optical phenomenon in chromium nanostructures.

Canfield and coworkers[21,22] found a huge shift of peaks in the extinction spectra for two different polarizations of V-shaped gold nanoparticles. Thus, the plasmon resonance depends on the shapes of the nanostructures. A V-shaped structure produces an artificial broken symmetry in the direction between its two arms within the substrate plane. For the second-order nonlinear optical response, noncentrosymmtric structures such as V shapes should lead to a high SHG intensity because of the sensitivity to the symmetry of SHG signals. Thus, V-shaped nanoholes formed periodically can be utilized to survey the response of the plasmon resonance to this additional broken symmetry on a planar sample of chromium metal. The response should be seen in the measured second-order nonlinear susceptibility tensor elements. It is noted that Cr metal has good adhesion to the substrate. To make very small V-shaped nanoholes, a very thin and uniform film is needed, and Cr is the best material[23]. Technologically, therefore, it is most interesting to be able to control the nonlinear optical behavior of Cr nanostructures for an optical device on a chip[23].

In our study, we investigated the nonlinear susceptibility properties of V-shaped subwavelength slits formed in a 15-nm-thick chromium film fabricated by electron beam lithography. We measured the azimuthal angular dependence of the SHG from the sample for different input and output polarization combinations. The decomposed nonlinear susceptibility element $\chi_{313}^{(2)}$ should contain the field

enhancement effect at the sharp apex. We will discuss whether the plasmon contribution is dominant or not on the basis of the susceptibility elements obtained.

2. Experimental procedure

The silica substrate was first coated with 15 nm Cr by evaporation and then cut into small pieces of 12 x 12 mm^2. The sample was then spin-coated with a 40 nm e-beam resist and patterned by e-beam lithography using a 100 keV acceleration voltage, a 200 pA beam current, and a dose of 150 $\mu C/cm^2$. After resist development, the patterns were then transferred to Cr using dry etch processes before removing the resist completely. The V-shaped apertures are schematically depicted in Fig. 1(a). The V-shaped apertures are 150 nm in length and 50 nm wide, have a 360 nm periodicity, and the angle of the apex is 120^o. Indeed, V-shaped structural parameters such as arm length, arm width, apex angle, and periodicity were modified to probe the SHG response. The V-shaped nanohole structural parameters used in this study produced the strongest anisotropic behaviour in second harmonic generation response. The whole array covered an area of about 100 μm^2. An atomic force microscopy image of the fabricated structures is shown in Fig. 1(b).

As the excitation source of the SHG from the sample, we used the second harmonic denoted ω of a mode-locked Nd:YAG picosecond laser. Its output pulse width was 30 ps and the repetition rate was 10 Hz. For measuring the azimuthal angle dependence of the SHG, the sample was mounted on an automatic rotation stage. The incident polarized light at the photon energy of 2.33 eV illuminated the V-shaped area at an angle of 45^o with respect to the surface normal. Direction 3 is defined as the

direction normal to the surface while directions 1 and 2 are on the sample surface. 1 indicates the direction of the bisector of the V passing through its apex in the substrate plane. Azimuthal angle φ is defined as the angle between the incident plane and direction 1. At zero degrees, the fundamental light first illuminates the nanohole arrays at the valley between the two arms of the V-shaped structure. The inset at the center of Fig. 2 illustrates the relative position between the incident plane and direction 1. After passing through a polarizer, a focusing lens, and a 2ω cut filter, a laser spot of 1 mm diameter was focused on the V-shaped area. To ensure that the laser beam always illuminated the V-shaped nanoholes during the rotation of the stage, care was taken that both the laser spot and the V-shaped area were on the rotation axis. To avoid damaging the sample, the average energy of the incoming beam was kept at about 30 μJ/pulse. The reflected radiation at the doubled frequency 2ω was passed through an ω cut filter, an analyzer, and a focus lens and was detected by a photomultiplier through a monochromator. SHG signals for 10^4 laser shots were accumulated for each data point in Fig. 2. All measurements were carried out at room temperature and in air.

3. Results and discussion

Figures 2(a)-2(d) show the SHG signals from V-shaped subwavelength nanoholes for four different input and output polarization combinations, Pin/Pout, Pin/Sout, Sin/Pout, and Sin/Sout, at the fundamental photon energy of 2.33 eV. The filled circles show the experimental data and the solid lines show the results calculated by a least-squares fitting program based on the model below. The relative scale is an arbitrary unit of

SHG intensity and is shown at the upper right corner of each "radar" chart. The anisotropy of the signal indeed reflects the structural anisotropy of the V-shaped nanohole arrays. Namely, both the SHG signal pattern shapes and the fabricated V-shapes show a mirror symmetry with respect to the line including the $\varphi=0^{o}$ and 180^{o} directions. As a control, Figs. 2(e)-2(h) show SHG signals from a bare chromium substrate. Only a weak dependence of SHG signal intensity on the rotation angle is seen in Figs. 2(e)-2(h).

Following the theoretical approach performed by Omote et al.[24], we analyzed the SHG intensity patterns from the V-shaped holes in Figs. 2(a)-2(d). In doing so, the V-shaped nanohole array was treated as a flat thin dielectric slab with a thickness *d* of 5 nm and the dielectric constants of chromium at ω and 2ω frequencies quoted from Palik's handbook[25]. The induced nonlinear polarization in the second layer was defined as

$$P_i(2\omega) = \varepsilon_o \chi^{(2)}_{ijk} : E_i(\omega) E_j(\omega). \quad (1)$$

Here, ε_o is the permittivity of the vacuum, and E_i and E_j are the two applied electric fields at frequency ω. Since V-shaped nanoholes have C_s symmetry, ten independent nonlinear susceptibility elements, $\chi^{(2)}_{223}$, $\chi^{(2)}_{113}$, $\chi^{(2)}_{212}$, $\chi^{(2)}_{122}$, $\chi^{(2)}_{111}$, $\chi^{(2)}_{133}$, $\chi^{(2)}_{313}$, $\chi^{(2)}_{322}$, $\chi^{(2)}_{311}$, and $\chi^{(2)}_{333}$, are permitted[26]. The solid curves in Figs. 2(a)-2(d) show the calculated SHG intensity patterns. Pearson's correlation coefficients are r = 0.79 for (a), r = 0.28 for (b), r = 0.47 for (c), and r = 0.36 for (d).

Figure 3 shows the calculated SHG intensity patterns of V-shaped Cr nanoholes when one of the surface nonlinear susceptibility elements is set equal to the calculated value and all the other elements are set equal to zero. Consider in particular the

Pin/Pout configuration because the r factor 0.79 shows a strong correlation[27] between the experimental data and the theoretical fit. The SHG intensities of the $\chi^{(2)}_{322}$ and $\chi^{(2)}_{333}$ elements exceed those of the others in the Pin/Pout configuration. The contribution of $\chi^{(2)}_{313}$ and $\chi^{(2)}_{311}$ components makes the intensity in the Pin/Pout configuration higher at an angle of $\varphi=180^{o}$, as shown in Figs. 3 and 2(a).

We also tried to fit the theoretical SHG intensity patterns to the experimental data in Figs. 2(e)-2(h) by assuming C_∞ symmetry for the bare Cr substrate. Under the C_∞ symmetry, there are three independent nonlinear susceptibility elements, $\chi^{(2)}_{113}$ ($=\chi^{(2)}_{223}$), $\chi^{(2)}_{311}$ ($=\chi^{(2)}_{322}$), and $\chi^{(2)}_{333}$. The SHG intensity contributions from $\chi^{(2)}_{311}$ and $\chi^{(2)}_{333}$ were predominant in the Pin/Pout configuration.

As for the origins of $\chi^{(2)}_{311}$ and $\chi^{(2)}_{333}$ elements, it is impossible to distinguish between the contribution of the V-shaped Cr nanoholes and the bare Cr substrate since these two susceptibility elements appear simultaneously under C_s (V-shaped hole) and C_∞ (bare Cr substrate) symmetries. On the other hand, the contribution of the nonlinear susceptibility element $\chi^{(2)}_{313}$ in Fig. 3 should be purely from the nanoholes because it emerges owing to the symmetry breaking in direction 1 created by the V-shaped nanoholes.

To understand the physical origin of the large contribution of the $\chi^{(2)}_{313}$ element, we discuss several competing candidate origins including edge nonlinearity, plasmon exciation, "lightning rod effect"[28], and bulk quadrupoles. The first candidate origin is the contribution of the edge nonlinearity in the $\chi^{(2)}_{313}$ element. We define the edge nonlinearity as that from the vertical metallic sidewalls in each V-shaped hole. If the

nonlinear polarization emitted from the metallic sidewalls is in direction 3, then it might contribute to the macroscopic $\chi^{(2)}_{313}$ element. In principle, the total nonlinear polarization $P(2\omega)$ must be proportional to the area of the vertical metallic sidewalls. However, our rough calculation shows that the area ratio between the exposed Cr metal of the sample surface to that of the vertical sidewalls in the nanoholes sample is 10^6:1. The SHG signal intensity of the sidewalls thus should be much lower. Consequently, the contribution of the edge nonlinearity is hardly feasible as the origin of the nonlinear susceptibility element $\chi^{(2)}_{313}$.

The next step is to discuss plasmon excitation and the "lightning rod effect" at the sharp apex[14] between two V-shaped arms. These two candidate origins should be considered together because the "lightning rod effect" and the localized field enhancement by the surface plasmon resonances have similar behaviours[29]. When we consider the local field enhancement at the fundamental and second harmonic frequencies, the effective nonlinear susceptibility $\chi^{(2)}_{313,\mathrm{eff}}$ can be expressed as[30]

$$L_3(2\omega).\chi^{(2)}_{313}.L_1(\omega).L_3(\omega) \rightarrow \chi^{(2)}_{313,\mathrm{eff}} \quad (2)$$

Here, $L_1(\omega)$ and $L_3(\omega)$ are the local field factors at the fundamental frequency. $L_3(2\omega)$ indicates the local field factor at the second harmonic frequency. If the surface plasmon resonance or "lightning rod effect" contributes to Eq. (2), a large local field factor $L_1(\omega)$ or $L_3(\omega)$ is interpreted as making a strong nonlinear polarization in directions 1 and 3. If so, the contributions of the nonlinear susceptibility elements $\chi^{(2)}_{311}$ and $\chi^{(2)}_{322}$ in Fig. 3 would differ strongly because the nonlinear polarization caused by $\chi^{(2)}_{311}$ and $\chi^{(2)}_{322}$ elements is proportional to the second

power of the local field factor $L_1(\omega)$ and $L_2(\omega)$, respectively. This is not the case because the ratio $I_{\chi^{(2)}_{311}}/I_{\chi^{(2)}_{322}}$ in Fig. 3 is 1.05. This implies that the local field enhancement at the apex is not significant.

Another noticeable feature of V-shaped Cr nanoholes is that nonlinear susceptibility elements $\chi^{(2)}_{122}$ and $\chi^{(2)}_{212}$ were absent. For V-shaped Au nanoparticles, these two nonlinear susceptibility elements presented a predominant enhancement caused by the plasmon resonance. More precisely, in the case of the $\chi^{(2)}_{122}$ element of Au nanoparticles, the applied electric field is in direction 2. High-order plasmonic waves were formed and propagated on the surface of these V-shaped gold nanoparticles. They created a strong electric field at the ends, at the middles, and at the intersection of the two arms. These "hot spots" act as the source of SHG and emit the nonlinear polarization in direction 1. In the same way, the applied electric field is in direction 1 in the case of the $\chi^{(2)}_{212}$ element. The "hot spot" was created at the intersection of the two arms and nonlinear polarization was emitted in direction 2[22,31].

The last candidate origin is the contribution of the electric quadrupole and magnetic dipole to the second harmonic generation. In general, we can express this higher-order contribution into the nonlinear polarization at 2ω as[29,32]

$$P_i^{bulk}(2\omega) \propto \Gamma_{ijkl} \vdots E_j(\omega)\nabla_k E_l(\omega). \quad (3)$$

Here, Γ_{ijkl} is the third rank susceptibility tensor. $E_j(\omega)$ and $E_l(\omega)$ are the two applied electric fields at frequency ω. Because the Cr metal was deposited by e-beam evaporation on the silica substrate, it can be determined to have isotropic symmetry, and 21 nonzero bulk nonlinear susceptibility elements (Γ_{ijkl}) are permitted[33,34]. When

the nonlinear polarization is along direction 3, the Γ_{ijkl} becomes Γ_{3jkl}. That is, Γ_{3333}, Γ_{3311} (= Γ_{3322}), Γ_{3131} (= Γ_{3232}), and Γ_{3113} (= Γ_{3223}) show the bulk nonlinear susceptibility elements.

It is often said that the bulk quadrupoles' contribution is weaker than the surface dipole contribution[35,36]. However, this is not the case for nanomaterials, because we cannot distinguish between their surface and bulk contributions. Thus, this candidate remains and there are similar examples[29,37]. As for the $\chi^{(2)}_{313}$ element, two applied electric fields are polarized in directions 1 and 3 and the higher-order contribution can be written as

$$P_3^{bulk}(2\omega) \propto \Gamma_{3311} E_3(\omega) \nabla_1 E_1(\omega) + \Gamma_{3113} E_1(\omega) \nabla_1 E_3(\omega). \quad (4)$$

As mentioned above, there are vertical metallic sidewalls contained within each V-shaped hole and they have air-chromium metal boundaries. This has a strong effect on the gradient operator ∇_1 because of the rate of spatial change of the field at the boundary of the nanohole surface. If we take the integration over the perimeter of all V-shaped holes, the nonlocal contribution thus may yield a considerable contribution.

We should also interpret the stronger contribution of the nonlinear susceptibility elements $\chi^{(2)}_{322}$, $\chi^{(2)}_{311}$, and $\chi^{(2)}_{333}$ in Fig. 3, which start with subscript number "3". This implies that the induced second-order polarization perpendicular to the metal surface occurs more efficiently than that parallel to the surface. This is because of the image dipole effect[38-40]. The dielectric function of Cr metal is -4.26+i 3.76 at 266 nm. Since the real part of the dielectric function is negative, the image dipole effect is possible.

The source of the fluctuation in Fig. 2 can be sample imperfections, such as fabrication errors, surface roughness, and dust. For e-beam lithography, there tends to be a small deviation from the ideal shape[22,41,42]. Owing to the surface roughness of Cr metal, the measured point by SHG on the substrate may microscopically move as the sample is rotated[43]. Tiny dust particles were probably attached on the sample surface during the measurements in air and are unavoidable. Most importantly, the $\chi_{313}^{(2)}$ element emerged only in the zone where the V-shaped nanoholes were located and not on the bare Cr substrate. This means that dust does not exert significant effects on the $\chi_{313}^{(2)}$ element because in the end the random dust effects tend to average out.

4. Conclusions

We fabricated V-shaped subwavelength slits formed in a 15-nm-thick chromium film and detected their SHG signal response. The V-shaped nanoholes were found to induce the nonlinear susceptibility element $\chi_{313}^{(2)}$. The observed SHG response was attributed to the nonlocal bulk contribution of the Cr metal.

Acknowledgements

This work was supported in part by a Grant-in-Aid for Scientific Research (c) of the Japan Society for the Promotion of Science (#23540363). N. K. Quang thanks the Vietnamese Government for the 322 scholarship program. Professor Rutt thanks the Rank Prize Funds for support.

References

1) M. Kauranen and A. V. Zayats, Nat. Photonics **6**, 737 (2012).

2) W. Cai, U. K. Chettiar, A. V. Kildishev, and V. M. Shalaev, Nat. Photonics **1**, 224 (2007).

3) V. M. Shalaev, Nat. Photonics **1**, 41 (2007).

4) M. Gentile, M. Hentchel, R. Taubert, H. Guo, H. Giessen, and M. Fiebig, Appl. Phys B. **105**, 149 (2011).

5) V. K. Valev, A. V. Silhanek, N. Smisdom, B. De Clercq, W. Gillijns, O. A. Aktsipetrov, M. Ameloot, V. V. Moshchalkov, and T. Verbiest, Opt. Express **18**, 8286 (2010).

6) P. Biagioni, J. S. Huang, and B. Hecht, Rep. Prog. Phys. **75**, 024402 (2012).

7) H. Husu, B. K. Canfield, J. Laukkanen, B. Bai, M. Kuittinen, J. Turunen, and M. Kauranen, Metamaterials **2**, 155 (2008).

8) A. Boltasseva and V. M. Shalaev, Metamaterials **2**, 1 (2008).

9) M. Airola, Y. Liu, and S. Blair, J. Opt. A: Pure Appl. Opt. **7**, 118 (2005).

10) A. Lesuffleur, L. K. Kumar, and R. Gordon, Appl. Phys. Lett. **88**, 261104 (2006).

11) J. A. H. van Nieuwstadt, M. Sandtke, R. H. Harmsen, F. B. Segerink, J.C. Prangsma, S. Enoch, and L. Kuipers, Phys. Rev. Lett. **97**, 146102 (2006).

12) D. Sinton, R. Gordon, and A. G. Brolo, Microfluid Nanofluid **4**, 107 (2008).

13) F. Eftekhari and R. Gordon, IEEE J. Sel. Top. Quant. Electron. **14**, 1552 (2008).

14) A. Lesuffleur, L. K. S. Kumar, and R. Gordon, Phys. Rev. B. **75**, 045423 (2007).

15) C. Hubert, L. Billot, P. M. Adam, R. Bachelot, and P. Royer, Appl. Phys. Lett. **90**, 181105 (2007).

16) B. K. Canfield, S. Kujala, M. Kauranen, K. Jefimovs, and T. Vallius, Appl. Phys. Lett. **86**, 183109 (2005).

17) J. R. Sambles, G. W. Bradbery, and F. Yang, Contemp. Phys. **32**, 173 (1991).

18) D. Sarid and W. A. Challener, *Modern Introduction to Surface Plasmons Theory, Mathematica Modeling and Applications* (Cambridge University Press, New York, 2010) p. 283.

19) A. Shalabney, A. Lakhtakia, I. Abdulhalima, A. Lahav, Christian Patzig, I. Hazek, A. Karabchevsky, B. Rauschenbach, F. Zhang, and J. Xu, Photonics Nanostruct.: Fundam. Appl. **7**, 176 (2009).

20) H. A. Atwater, S. Maier, A. Polman, J. A. Dionne, and L. Sweatlock, MRS Bull. **30**, 385 (2005).

21) B. K. Canfield, S. Kujala, K. Jefimovs, T. Vallius, J. Turunen, and M. Kauranen, J. Opt. A: Pure Appl. Opt. **7**, 110 (2005).

22) B. K. Canfield, S. Kujala, K. Jefimovs, Y. Svirko, J. Turunen, and M. Kauranen, J. Opt. A: Pure Appl. Opt. **8**, 278 (2006).

23) A. D. Rakic, A. B. Djurisic, J. M. Elazar, and M. L. Majewski, Appl. Opt. **3**, 5271 (1998).

24) M. Omote, H. Kitaoka, E. Kobayashi, O. Suzuki, K. Aratake, H. Sano, G. Mizutani, W. Wolf, and R. Podloucky, J. Phys.: Condens. Matter. **17**, 175 (2005).

25) D. Edwards, *Handbook of Optical Constants of Solids*, ed. E. Palik (Academic Press, New York, 1985) p. 378.

26) P. Guyot-Sionnest, W. Chen, and Y. R. Shen, Phys. Rev. B **33**, 8254 (1986).

27) O. Wälder, *Mathematical Methods for Engineers and Geoscientists* (Springer, Germany, 2008) p. 99.

28) D. P. Fromm, A. Sundaramurthy, P. J. Schuck, G. Kino, and W. E. Moerner, Nano Lett. **4**, 957 (2004).

29) V. K. Valev, X. Zheng, C. G. Biris, A. V. Silhanek, V. Volskiy, B. De Clercq, O. A. Aktsipetrov, M. Ameloot, N. C. Panoiu, G. A. E. Vandenbosch, and V. V. Moshchalkov, Opt. Mater. Express **1**, 36 (2011).

30) T. Kitahara, A. Sugawara, H. Sano, and G. Mizutani, Appl. Surf. Sci. **219**, 271 (2003).

31) H. Husu, J. Mäkitalo, J. Laukkanen, M. Kuittinen, and M. Kauranen, Opt. Express **18**, 16601 (2010).

32) E. Kobayashi, G. Mizutani, and S. Ushioda, Jpn. J. Appl. Phys **36**, 7250 (1997).

33) R. L. Sutherland, *Handbook of Nonlinear Optics* (Marcel Dekker, New York, 2003) 2nd ed., p. 27.

34) R. W. Boyd, *Nonlinear Optics* (Academic Press, San Diego, 2003) 2nd ed., p. 51.

35) H. Tuovinen, M. Kauranen, K. Jefimovs, P. Vahimaa, T. Vallius, J. Turunen, N. V. Tkachenko, and H. Lemmetyinen, Nonlinear Optic. Phys. Mat. **11**, 421 (2002).

36) F. X. Wang, F. J. Rodríguez, W. M. Albers, R. Ahorinta, J. E. Sipe, and M. Kauranen, Phys. Rev. B. **80**, 233402 (2009).

37) R. Zhou, H. Lu, X. Liu, Y. Gong, and D. Mao, J. Opt. Soc. Am. B **27**, 2405 (2010).

38) S. F. A. Kettle, Spectrochimica Acta Part A **54**, 1639 (1998).

39) K. G. Lee, K. J. Ahn, H. W. Kihm, J. S. Ahn, T. K. Kim, S. Hong, Z. H. Kim, and D. S. Kim, Opt. Express **16**, 10641 (2008).

40) A. Kudelski, Vibrational Spectroscopy **39**, 200 (2005).

41) N. Meinzer, M. Wegener, M. F. G. Klein, P. J. Jakobs, H. Hein, M. König, J. Niegemann, K. Busch, N. Feth, and S. Linden, Conference on Quantum Electronics and Laser Science. CLEO/QELS, 2008, p. 1.

42) M. F. G. Klein, H. Hein, P. J. Jakobs, S. Linden, N. Meinzer, M. Wegener, V. Saile, and M. Kohl, Microelectron. Eng. **86**, 1078 (2009).

43) N. A. Tuan and G. Mizutani, e-J. Surf. Sci. Nanotech. **7**, 831 (2009).

Figure captions

Fig. 1. (Color online) Structure of V-shaped subwavelength nanohole array: (a) scheme of the designed parameters and (b) atomic force microscopy image.

Fig. 2. (Color online) Polar plots of second harmonic generation intensity (filled circles) versus azimuthal angle φ from V-shaped nanoholes (a-d) and bare Cr substrate (e-h) at the fundamental photon energy of 2.33 eV and an incident angle of 45^{o}. The relative scale is an arbitrary unit of SHG intensity, shown at the upper right corner of each radar chart. The solid lines are the best-fit theoretical patterns calculated with nonlinear susceptibility $\chi_{ijk}^{(2)}$ elements as adjustable parameters. The inset at the center defines the azimuthal angle φ in relation to the coordinate. At zero degrees, the fundamental light illuminates the nanohole arrays at the valley between two arms of the V-shaped structure.

Fig. 3. Decomposition of SHG intensity from V-shaped nanoholes when one of the nonlinear susceptibility elements $\chi_{ijk}^{(2)}$ is set equal to a calculated value and all the other elements are set equal to zero. The intensities are arbitrary but on a common scale. ijk are the suffices of the nonlinear susceptibility elements.

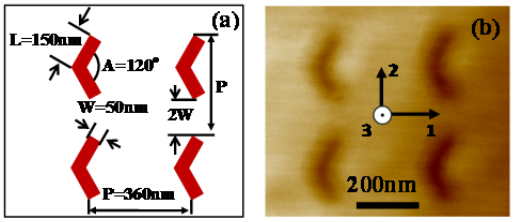

Fig. 1

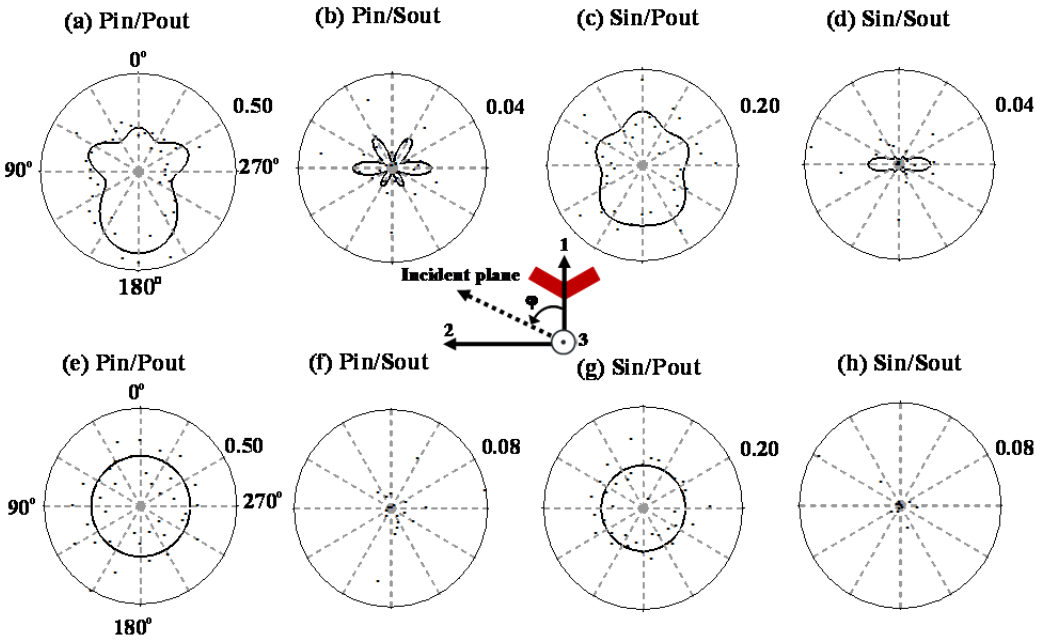
(a) Pin/Pout
(b) Pin/Sout
(c) Sin/Pout
(d) Sin/Sout
0°
90°
270°
180°
0.50
0.04
0.20
0.04
Incident plane
φ
1
2
3
(e) Pin/Pout
(f) Pin/Sout
(g) Sin/Pout
(h) Sin/Sout
0°
90°
270°
180°
0.50
0.08
0.20
0.08

Fig. 2

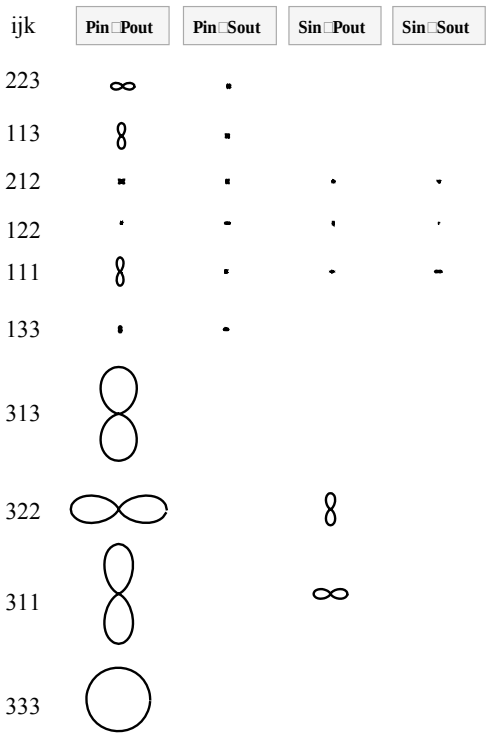
ijk
Pin□Pout
Pin□Sout
Sin□Pout
Sin□Sout
223
113
212
122
111
133
313
322
311
333

Fig. 3